

Structure and Composition of Silicon Carbide Films Synthesized by Ion Implantation

K. Kh. Nussupov, N. B. Beisenkhanov*, S. K. Zharikov, I. K. Beisembetov, B. K. Kenzhaliev, T. K. Akhmetov, and B. Zh. Seitov

Kazakh–British Technical University, Tole bi 59, Almaty, 050000 Kazakhstan

* e-mail: n.beisenkhanov@kbtu.kz

Received March 5, 2014; in final form, June 10, 2014

Abstract—The mathematical decomposition of the IR absorption spectrum obtained from a Si layer after the C⁺ ion implantation with an energy of 10 or 40 keV or from a homogeneous SiC_{0.7} film has demonstrated that fractions of weak elongated Si–C bonds in the amorphous phase, strong shortened Si–C bonds on the surface of small nanocrystals, and tetrahedral Si–C bonds in the crystalline phase (degree of crystallinity) after high-temperature annealing (1250–1400°C) of the layers are equal to 29/29/42, 22/7/71, and 21/31/48%, respectively. A system of SiC_{2.0}, SiO₂, SiC_{0.8}, and SiC_{0.6} layers in the film on the Si substrate has been identified using X-ray reflectometry and the simulation with the Release software. The reflectometry data on fluctuations of the intensity of X-ray reflections in the region of the main maximum have been interpreted in terms of variations in the density over the depth of the layer with a Gaussian distribution of carbon atoms from 2.55 and 2.90 g/cm³ for the SiC_{0.25} and SiC_{0.65} layers, respectively, to 3.29 g/cm³ for the SiC_{1.36} layer.

DOI: 10.1134/S1063783414110237

1. INTRODUCTION

Owing to valuable physicochemical properties (wide band gap $E_g = 2.3\text{--}3.5$ eV, high hardness and chemical resistance, high charge carrier mobility, and possibility of synthesizing materials with electron and hole conductivities), silicon carbide has been widely used in optoelectronics; high-frequency, high-temperature, and radiation resistant electronics, etc. [1–3]. Electronic devices based on SiC can operate at temperatures up to 600°C and possess high-speed response and radiation resistance [4, 5]. The ion implantation synthesis of SiC layers in silicon makes it possible to obtain films of specified thickness and composition [6–11].

Silicon carbide exhibits blue emission at low temperatures [12]. Since SiC is a wide-band-gap semiconductor with an indirect band gap, the use of this material in light-emitting devices is complicated. Owing to the increased interest in silicon-based materials emitting in the blue range, the synthesis of SiC nanocrystals embedded in SiO₂ films by ion implantation has gained significant importance [12–14]. The double implantation of Si⁺ and C⁺ ions into a SiO₂ matrix leads to a change in properties of silicon nanocrystals and to the formation of a system containing nanoinclusions of carbon, silicon, and silicon carbide, which, due to the quantum confinement effect, provide luminescence in almost the entire visible spectral region [12, 13, 15–17]. In particular, Tetelbaum et al. [13] performed implantation of Si⁺ and C⁺ ions with an

energy $E = 100$ keV and a dose $D = 7 \times 10^{16}$ cm⁻² into the SiO₂ film so that the excessive concentrations of Si and C ions at the maximum of their distribution reached 10 at %. The white photoluminescence observed by these authors is characterized by three bands at ~400, ~500, and ~625 nm, which are assigned to nanoinclusions of SiC phases, C nanoclusters (*ncI*), and small Si nanocrystals (*nc*), respectively. This field of investigation is promising for the design and fabrication of light-emitting diodes, lasers, planar optical amplifiers, and others.

The high rate of increase in the efficiency of devices is associated with the transition to the third-generation silicon photoelectric converters, which are based on multilayer and multibarrier structures, including materials with different band gaps E_g . This makes it possible to decrease the losses in the crystal due to both the impossibility of absorbing photons with energies less than the band gap E_g of the crystal and the thermalization of the crystal lattice upon absorption of photons with energies greater than the band gap and to exceed the theoretical limit of the photovoltaic energy conversion by 27% for single-crystal silicon [18, 19]. The thermalization can be decreased using a wider-band-gap material, as compared to silicon, in multilayered structures. This material can be a wide-band-gap SiC layer or a layer with silicon nanocrystals, in which the band gap E_g is determined by quantum confinement effects and can significantly exceed the band gap E_g of bulk single-crystal silicon. The use of these

materials makes it possible to extend the region of spectral sensitivity of silicon photoelectric converters to the shorter wavelength part of the solar radiation spectrum [19].

Microcrystalline alloys $\mu\text{c-SiC} : \text{H}$ are promising materials for the use as transparent conductive window layers in thin-film solar cells. They have a high n -type conductivity and a wide optical band gap. Owing to these properties, $\mu\text{c-SiC} : \text{H}$ is used as the window layer in n -side illuminated single-junction microcrystalline silicon ($\mu\text{c-SiC} : \text{H}$) solar cells [20, 21]. Ogawa et al. [22] reported on the fabrication of $n-i-p$ -type amorphous silicon ($a\text{-Si} : \text{H}$) thin-film solar cells using phosphorus-doped microcrystalline cubic silicon carbide ($\mu\text{c-3C-SiC} : \text{H}$) films as a window layer. The solar cell had the following configuration: TCO (transparent conductive oxide)/ TiO_2/n -type $\mu\text{c-3C-SiC} : \text{H}/\text{intrinsic } a\text{-Si} : \text{H}/p$ -type $\mu\text{c-SiC}_x(a\text{-SiC}_x : \text{H}$, including $\mu\text{c-Si} : \text{H}$ phase)/Al. The characteristics of the solar cell were as follows: the efficiency was 4.5%, and the open-circuit voltage was $V_{\text{oc}} = 0.953$ V. These authors also prepared a solar cell with the undoped $a\text{-Si}_{1-x}\text{C}_x : \text{H}$ film as a buffer layer to improve the n/i interface. The open-circuit voltage was $V_{\text{oc}} = 0.966$ V.

Amorphous silicon carbide is also a promising material for the use in solar power engineering. For example, a boron-doped hybrid amorphous silicon carbide/nanocrystalline silicon (p -type $a\text{-SiC}/nc\text{-Si}$) window layer prepared by Ma et al. [23] has a great potential to improve the solar cell performance due to the wide optical band gap, high charge carrier mobility, and high doping efficiency. A thin (< 30 nm) high-quality hybrid p -type $a\text{-SiC}/nc\text{-Si}$ window layer with controllable nano-sized silicon crystals embedded in the amorphous silicon carbide matrix was prepared by radio-frequency plasma-enhanced chemical vapor deposition (RF-PECVD) at 150°C . The layer had a large optical band gap (~ 2.2 eV). A high open-circuit voltage of more than 0.96 V and a high quantum efficiency in the short-wavelength region were achieved for the $n-i-p$ -type $a\text{-Si}$ single-junction solar cell. Pysch et al. [24] fabricated and investigated the emitter system consisting of an n -doped hydrogenized amorphous silicon carbide $a\text{-SiC} : \text{H}(n)$ layer with or without a pure hydrogenized intrinsic amorphous silicon $a\text{-Si} : \text{H}(i)$ intermediate layer. The highest efficiency of solar cells reached 18.5%.

Klyui et al. [25] showed that silicon carbide antireflection coatings can improve the efficiency of solar cells up to 1.3 times. The deposition of diamond-like carbon antireflection coatings also makes it possible to improve the efficiency of solar cells by a factor of 1.35–1.50 [25]. The improvement is associated with the decrease in reflection losses and with the passivation of active recombination centers.

Thus, SiC and Si nanocrystals can be used to increase the efficiency of solar cells. Naturally, the question arises as to which distribution profile of

implanted carbon atoms in silicon or SiO_2 is the most preferred when using ion implantation. This can be an inhomogeneous or Gaussian distribution profile of implanted atoms over the depth [6, 8, 9, 26–38]. Then, we can expect a change over the depth not only in the concentration of C and Si atoms but also, as a consequence, in the concentration of nanocrystals and nanoclusters of Si, SiC, and C after annealing. This can offer certain advantages in the generation of white luminescence from SiO_2 layers or hybrid window layers of solar cells, because the ion-implanted layer consists of nanolayers containing a wide variety of nanocrystals and nanoclusters that differ from each other in the type and size of the nanoparticles. On the other hand, the layer prepared by multiple implantation of ions with different energies into the substrate can have a homogeneous [6, 29, 32, 39–43] (rectangular) distribution profile of C and Si atoms over the depth. Such a layer can contain desired types of nanoparticles with specific sizes and concentrations. It is a convenient object for investigation and application. In this case, the fraction of SiC nanocrystals in the total SiC volume is of particular importance. The composition of the implanted layer can be predicted based on reliable information about the influence of the concentration of components and the annealing temperature on the formation of nanocrystals and nanoclusters of C, Si, and SiC.

In this work, we synthesized homogeneous and inhomogeneous SiC films with different (rectangular and Gaussian) distribution profiles of carbon atoms over the depth of the impurity by the implantation of $^{12}\text{C}^+$ ions into silicon. We investigated the influence of the distribution of carbon atoms in silicon on the phase composition and the degree of crystallinity of the layer and on the formation of SiC nanocrystals during the annealing. A quantitative estimate was obtained for the volume ratio of the crystalline and amorphous phases of silicon carbide in implanted layers.

2. SAMPLE PREPARATION AND EXPERIMENTAL TECHNIQUE

Carbon ions were implanted into single-crystal Si(100) plates $7 \times 7 \times 0.3$ mm in size with an electrical resistivity of 4–5 Ω cm [10, 11]. In order to prevent heating of the sample above 25°C , the accelerator current density did not exceed $3 \mu\text{A}/\text{cm}^2$. We synthesized inhomogeneous SiC films with a Gaussian distribution of carbon atoms (with energies of 10 and 40 keV during the implantation) in silicon and homogeneous $\text{SiC}_{0.7}$ films (rectangular distribution profile) on silicon by the multiple $^{12}\text{C}^+$ implantation with different ion energies (40, 20, 10, 5, and 3 keV) in silicon.

The composition and structure of the films were investigated using IR spectroscopy on a Thermo Scientific Nicolet iS50 FT-IR spectrometer (United States). The software program for the Nicolet iS50

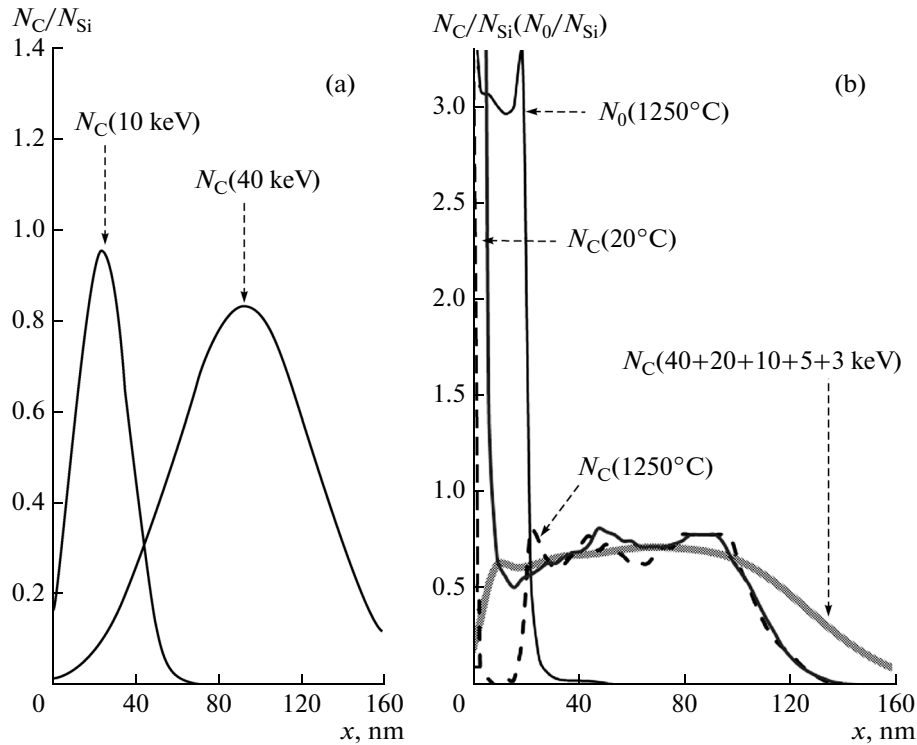


Fig. 1. Calculated implantation profiles of the ^{12}C distribution in silicon, constructed according to Gibbons et al. [46] for the parameters E , D , $R_p(E)$, and $\Delta R_p(E)$ given in Table 1: (a) Gaussian distribution profiles $N_C(10\text{ keV})$ and $N_C(40\text{ keV})$; (b) rectangular distribution profile $N_C(40 + 20 + 10 + 5 + 3\text{ keV})$ and Auger profiles of carbon and oxygen atoms in the layer $N_C(20^\circ\text{C})$ (after implantation at 20°C), $N_C(1250^\circ\text{C})$ (after annealing for 30 min at $T = 1250^\circ\text{C}$), and $N_0(1250^\circ\text{C})$ (after annealing for 30 min at $T = 1250^\circ\text{C}$).

spectrometer allows the use of modern programs on the decomposition of the IR absorption spectra into components.

The surface microstructure of the implanted layer was examined on a JEOL JSPM5200 atomic force microscope (Japan) using the semicontact method. The in-plane resolution of the microscope was 0.14 nm, and the vertical resolution was 0.01 nm.

The transmission electron microscopy (TEM) investigations were performed on a JEOL JEM-100CX transmission electron microscope (Japan) at an electron gun accelerating voltage of 100 kV. The morphology was examined predominantly using the bright-field method, when the structure of the samples was observed in the transmitted electron beam.

The density and thickness of the films were determined using X-ray reflectometry by recording the angular dependence of the reflectivity for two X-ray spectral lines CuK_α (0.154 nm) and CuK_β (0.139 nm) on the CompleXRay-C6 facility. The selection of the spectral lines CuK_α and CuK_β from the polychromatic spectrum was carried out using thin semitransparent and thick opaque pyrolytic graphite monochromators, respectively, with a mosaic angle of 0.5° [44, 45]. Using the computer simulation of the reflectometry

data, we can determine the composition, thickness, and density of the films.

The samples were annealed at temperatures of 1200, 1250, 1300, or 1400°C for 30 min in a vacuum or in an argon atmosphere with a low O_2 content.

3. RESULTS

3.1. Ion Implantation Synthesis of Inhomogeneous Films of Silicon Carbide SiC in Silicon and Investigation of Their Characteristics

We calculated and constructed the profiles of carbon atom distribution over the depth of the Si substrate for the implantations of carbon ions with the parameters $E = 40\text{ keV}$, $D = 3.56 \times 10^{17}\text{ cm}^{-2}$ and $E = 10\text{ keV}$, $D = 1.56 \times 10^{17}\text{ cm}^{-2}$. Figure 1 shows the calculated profiles N_C for the distributions of carbon atoms over the depth of the silicon substrate for these values of ion energies and doses (Table 1), which are the Gaussian distributions constructed according to the expression

$$N(x) = \frac{D}{\Delta R_p(2\pi)^{1/2}} \exp\left[-\frac{(x - R_p)^2}{2\Delta R_p^2}\right], \quad (1)$$

where x is the distance from the surface.

Table 1. Energies E , doses D , projected ranges $R_p(E)$, and root-mean-square deviations $\Delta R_p(E)$ [46] for $^{12}\text{C}^+$ ions in silicon, which are used in the construction of the Gaussian ($\text{SiC}_{0.84}$ and $\text{SiC}_{0.95}$ at the peak of the distribution) and rectangular ($\text{SiC}_{0.7}$ in the range of $\sim 8\text{--}100$ nm) distribution profiles

E , keV	$D(\text{SiC}_{0.84})$, 10^{17} cm^{-2}	$D(\text{SiC}_{0.95})$, 10^{17} cm^{-2}	$D(\text{SiC}_{0.7})$, 10^{17} cm^{-2}	N_C profile (Gibbons et al. [46])	
				$R_p(E)$, nm	$\Delta R_p(E)$, nm
40	3.56		2.80	93.0	34.0
20			0.96	47.0	21.0
10		1.56	0.495	24.0	13.0
5			0.165	12.3	7.0
3			0.115	7.5	4.3

The fraction of carbon atoms N_C/N_{Si} at the peak of the distribution is slightly less than the value corresponding to the stoichiometric SiC composition (Table 1). This makes it possible to avoid an excessive graphitization of the layer.

The distribution N_C/N_{Si} is constructed under the assumption that the concentration of Si atoms after the implantation does not significantly change over the depth and amounts to approximately the concentration of Si atoms in a silicon single crystal, i.e., $N_{\text{Si}} = 5 \times 10^{22} \text{ cm}^{-3}$. Indeed, the concentration of silicon atoms in a SiC single crystal does not significantly differ from this value and is equal to $4.83 \times 10^{22} \text{ cm}^{-3}$.

This assumption is important for the high-dose implantation of $^{12}\text{C}^+$ ions into silicon. It is based on the fact that the volume of the diamond-like unit cell of the silicon carbide SiC is approximately two times smaller than the volume of the silicon unit cell, and the high-dose carbon implantation is not accompanied by the processes of swelling of the layer due to the increase in the number of atoms. Of course, this assumption holds only under the condition $N_C < N_{\text{Si}}$.

The IR absorption spectrum of the silicon layer implanted with carbon ions (10 keV, $1.56 \times 10^{17} \text{ cm}^{-2}$) and annealed at a temperature of 1400°C for 30 min is shown in Fig. 2. The spectrum exhibits an intense peak

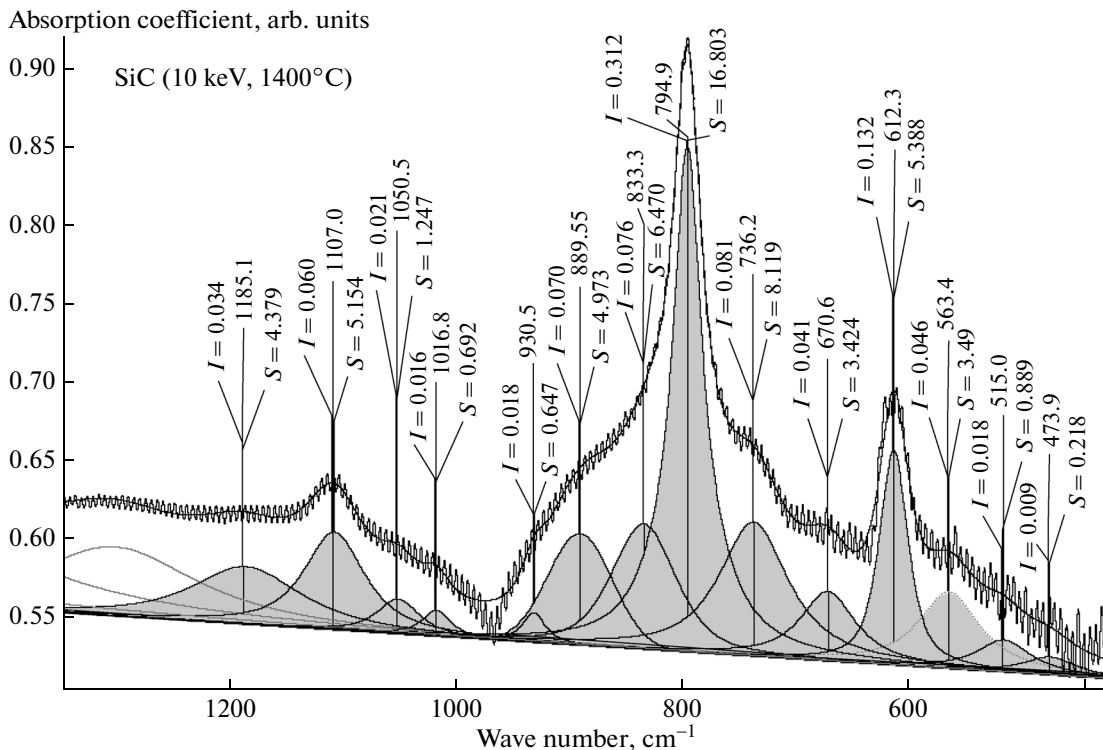


Fig. 2. Mathematical decomposition of the IR absorption spectrum of the silicon layer implanted with carbon ions (10 keV, $1.56 \times 10^{17} \text{ cm}^{-2}$) and annealed at 1400°C for 30 min (values at the points of the maxima of the peaks are their amplitudes I , positions, and areas S).

Table 2. Areas S and sums of the areas $\sum S$ for five components of the SiC peak and two components of the SiO peak at wave numbers w

Bond	$E = 10 \text{ keV}$				$E = 40 \text{ keV}$			
	$w, \text{ cm}^{-1}$	$S, \text{ arb. units}$	$S, \%$	$\sum S, \text{ arb. units}$	$w, \text{ cm}^{-1}$	$S, \text{ arb. units}$	$S, \%$	$\sum S, \text{ arb. units}$
Si–O (TO)	1107	5.15	80.5	6.4	1105.9	3.66	82.8	4.42
	1050.5	1.25	19.5	(100%)	1020.6	0.76	17.2	(100%)
Si–C (TO)	889.6	4.97	12.5	39.78 (100%)	887.1	1.68	4.3	39.07 (100%)
	833.3	6.47	16.3		853.3	0.86	2.2	
	794.9	16.8	42.2		793.1	27.88	71.4	
	736.2	8.12	20.4		742.6	7.18	18.4	
	670.6	3.42	8.6		671.6	1.47	3.8	
	612.3	5.39	100.0	5.39	612.2	7.29	100.0	7.29

of the crystalline SiC phase with the maximum at 794.9 cm^{-1} . After the mathematical decomposition, the IR absorption spectrum of the SiC layer is represented as the sum of 14 spectral components. For each component, we determined the position, area, and amplitude of the peak.

As can be seen from Fig. 2, there is a component with the maximum at 1107.0 cm^{-1} , which is associated with the presence of interstitial oxygen in the studied sample [47]. Lisovskyy et al. [48] showed that the main absorption band of the oxide can be represented as the sum of four profiles corresponding to the transverse optical stretching vibrations of the bridging oxygen involved in the composition of molecular complexes, such as SiOSi_3 (the component with the maximum at 995 cm^{-1}), SiO_2Si_2 (1033 cm^{-1}), SiO_3Si (1067 cm^{-1}), and SiO_4 (1100 cm^{-1}). The bands associated with longitudinal stretching vibrations of the Si–O bond are also due to the motion of bridging oxygen atoms involved in the composition of the complexes SiOSi_3 (1145 cm^{-1}) and SiO_2Si_2 (1205 cm^{-1}). The component with the maximum at 1107.0 cm^{-1} in Fig. 2 indicates that the SiO_4 complexes (1100 cm^{-1}) dominate in the oxide layer. It is also assumed that the oxide layer contains the molecular complexes SiO_3Si (1067 cm^{-1}) and SiO_2Si_2 (1033 cm^{-1}), which are responsible for the appearance of components with the closely spaced maxima at 1050.5 and 1016.8 cm^{-1} in the spectrum (Table 2).

Moreover, in the region between 590 and 630 cm^{-1} , there is a peak with the area $S = 5.39$ arb. units and with the maximum at a wave number of $\sim 612.3 \text{ cm}^{-1}$. This value is close to the wave number of 607 cm^{-1} , which is typical of substitutional carbon atoms [47]. The area of this peak varies within a narrow range (5–7 au) in c -Si single-crystal wafers with an electrical resistivity of $\sim 2000 \Omega \text{ cm}$, and the peak itself is assigned to carbon of the substrate material. However,

in [36], the local vibrational mode of substitutional carbon atoms was observed at 607 cm^{-1} for Si samples after the carbon ion implantation with an energy of 55 keV and a dose of $6 \times 10^{17} \text{ cm}^{-2}$, followed by the annealing at low temperatures (400°C); in this case, from 40 to 60% of the implanted carbon atoms occupied substitutional sites. Therefore, we cannot exclude the influence of carbon implanted into the subsurface layer on the area of the peak attributed to SiC, even though the area of this component was subtracted from the area of the SiC peak (Table 2).

Among the other components, noteworthy are the components at 736.2 and 670.6 cm^{-1} , which are characteristic of weak elongated Si–C bonds of amorphous silicon carbide; the component at 794.9 cm^{-1} , which is characteristic of tetrahedral Si–C bonds of crystalline SiC; and the components at 833.3 and 889.6 cm^{-1} , which are characteristic of shortened Si–C bonds that dominate on the surface of nanocrystals and in the clusters. From the ratio of the area of the component with the maximum at 794.9 cm^{-1} to the total area of the SiC peak (39.78 arb. units), we can estimate that approximately 42% of the total amount of SiC is contained in crystalline silicon carbide.

The structure of SiC films synthesized by ion implantation has been investigated in a large number of works. Nonetheless, the literature contains insufficient data on the quantitative estimation of the volume ratio between the crystalline and amorphous SiC phases. In particular, Kimura et al. [31] showed that, after the implantation of carbon ions ($E = 100 \text{ keV}$) into the n -Si(100) subsurface layers and the subsequent annealing at a temperature of approximately 900°C , the β -SiC phase contains 40–50% of the implanted carbon atoms, and, with an increase in the temperature to 1200°C , their amount increases to 70–80%. Kimura et al. [49] also showed that all the implanted carbon atoms are included in the β -SiC phase during the annealing at temperatures of 900 – 1200°C , if the concentration of carbon atoms does not

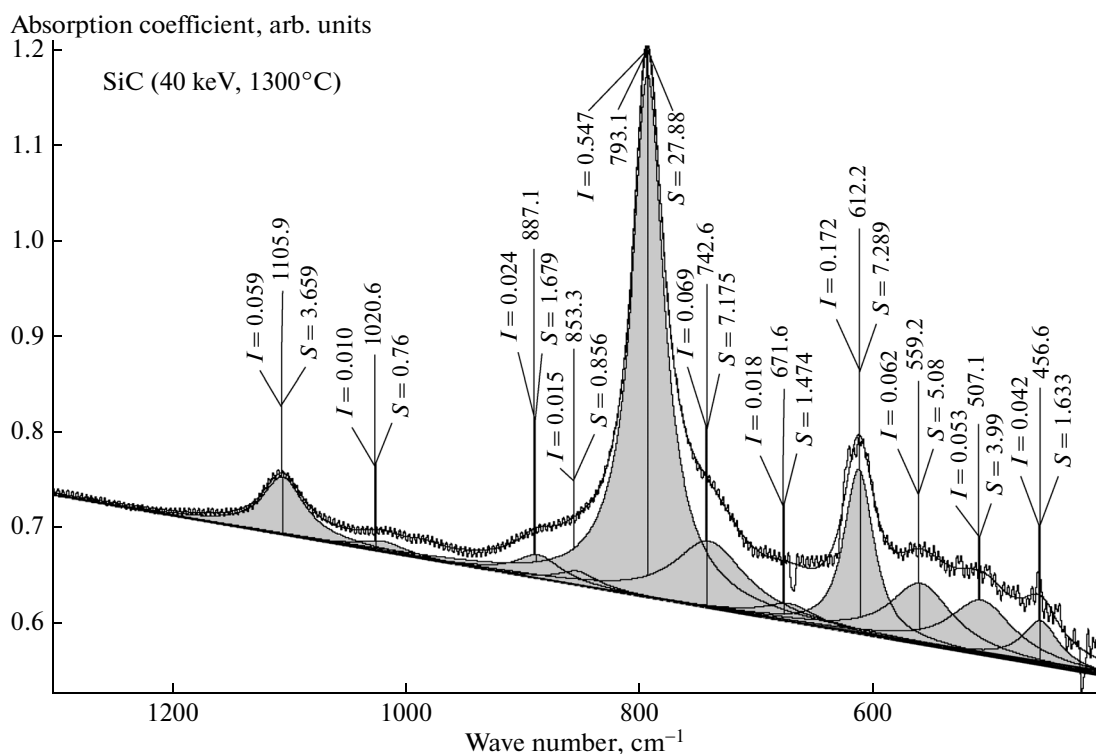


Fig. 3. Mathematical decomposition of the IR absorption spectrum of the silicon layer implanted with carbon ions (40 keV, $3.584 \times 10^{17} \text{ cm}^{-2}$) and annealed at 1300°C for 30 min (values at the points of the maxima of the peaks are their amplitudes I , positions, and areas S).

exceed their concentration corresponding to the stoichiometric β -SiC composition at the maximum of the distribution. At higher implantation doses, excess carbon atoms form clusters and are not embedded in β -SiC even after annealing at 1200°C.

Thus, it can be concluded that the low percentage (42%) of carbon inclusions in the crystalline SiC phase can indicate a high concentration of carbon and other carbon-containing clusters in the layer. This is quite probable, because, in the case of high-dose implantation of carbon ions with a low energy of 10 keV, we can expect that, in the subsurface layer (Fig. 1), the carbon concentration will increase to values higher than those corresponding to the stoichiometric composition due to both the effect of sputtering of the surface and the change in the composition of the layer. Indeed, the fractions of weak elongated Si–C bonds of the amorphous phase (components at 736.2 and 670.6 cm^{-1}), strong shortened Si–C bonds on the surface of small nanocrystals (components at 833.3 and 889.6 cm^{-1}), and tetrahedral Si–C bonds of the crystalline phase (degree of crystallinity) after high-temperature annealing at 1400°C are equal to 11.5/11.4/16.8 or 29/29/42%, respectively; i.e., a significant part of the amorphous phase (29%) is not included in the SiC nanocrystals, and the fraction of small SiC nanocrystals with shortened Si–C bonds (29%) on the surface is relatively high.

For example, Calcagno et al. [42] prepared $\text{Si}_{1-x}\text{C}_x$ alloys in silicon by multiple implantation of C^+ ions with doses in the range from 5×10^{16} to $3 \times 10^{17} \text{ cm}^{-2}$ and energies in the range of 10–30 keV. An increase in the carbon concentration ($x > 0.55$) leads to the appearance of carbon inclusions (with a characteristic size of 2.5 nm) in the sample. Yu Liangdeng et al. [6] revealed that the Raman spectra contain a doublet (1380 and 1590 cm^{-1}) due to graphitized amorphous carbon even after the implantation of carbon ions with an energy of 80 keV and a dose of $2.7 \times 10^{17} \text{ cm}^{-2}$ into silicon, when the carbon concentration at the maximum of the distribution was substantially below the concentration corresponding to the stoichiometric composition.

The IR absorption spectrum of the studied layer after the implantation (40 keV, $3.534 \times 10^{17} \text{ cm}^{-2}$) and annealing at 1300°C for 30 min is shown in Fig. 3. It can be seen that the spectrum contains a component with the maximum at 1105.9 cm^{-1} due to the presence of interstitial oxygen in the layer [47]. Also, there is a component that is characteristic of substitutional carbon with the maximum at 612.2 cm^{-1} , which almost coincides in position with the maximum corresponding to the layer prepared by the ion implantation with an energy of 10 keV but exceeds it in area ($S = 7.3$ and 5.4 arb. units). This can be explained by the larger

width of the SiC–Si transition layer due to the increase in values of R_p and ΔR_p (Table 1), specifically in the part near the substrate that can be considered as slightly defective.

From the ratio of the area of the components at 793.1 cm^{-1} to the total area of the SiC peak (39.07 arb. units), we can estimate that approximately 71% of the total amount of SiC is contained in crystalline silicon carbide; i.e., the degree of crystallinity is relatively high. In general, the ratio of weak elongated Si–C bonds (components at 742.6 and 671.6 cm^{-1}) of the amorphous phase, strong shortened Si–C bonds (components at 853.3 and 887.1 cm^{-1}) on the surface of small nanocrystals, and tetrahedral Si–C bonds of the crystalline phase (degree of crystallinity) is equal to $8.7/2.5/27.9$ or $22/7/71\%$. The content of the amorphous phase and, especially, the content of small nanocrystals are less than that for the layer implanted with 10-keV ions (29/29%) due to the lower concentration of carbon and, accordingly, other clusters in the layer.

For example, Wong et al. [50] synthesized the buried SiC layers by the carbon implantation into the p -Si(100) substrate using a MEVVA ion source with energies in the range of 30–60 keV and doses of $(0.3\text{--}1.6) \times 10^{18} \text{ cm}^{-2}$. The IR absorption spectra of the SiC layers after annealing at 700–1200°C were decomposed into two or three components, one of which was assigned to amorphous SiC and the other two were attributed to β -SiC. At a fixed dose, the total amount of SiC increases linearly with increasing implantation energy, whereas at a fixed energy, it increases as a fractional power of the dose, namely, D^y with the exponent $y = 0.41$. These data can be explained by the decrease in the concentration of carbon atoms and carbon clusters and, consequently, by the increase in the number of Si–C bonds with increasing energy and increasing range of ions at a fixed dose and by the increase in the number of carbon atoms and Si–C bonds with increasing dose at a fixed energy.

In our case, an increase in the energy and layer thickness by a factor of 4 and an increase in the ion dose by a factor of 2.3 should lead to a substantial increase in the number of Si–C bonds and, accordingly, to an increase in the area of the SiC peak. However, this does not occur, and the areas of the SiC peak after annealing are nearly equal to each other for the implantations of carbon ions with energies of 10 and 40 keV; i.e., they are 39.78 and 39.07 arb. units, respectively (Table 2). This can be associated with the fact that the annealing temperatures (1400 and 1300°C) near the melting point of silicon differ by 100°C. The annealing at 1400°C leads to an intensive decomposition of stable carbon clusters and to the formation of small SiC nanocrystals in the layer prepared by the implantation of ions with an energy of 10 keV, as well as to an increase in the total area of the SiC peak due to the increase in the number of shortened

Si–C bonds (833.3 and 889.6 cm^{-1}) with a small fraction of tetrahedrally oriented Si–C bonds (42.2%).

Hence, it follows that the thin (<30 nm) high-quality hybrid p -type a -SiC/ nc -Si window layer with controllable nano-sized silicon crystals embedded in the amorphous SiC matrix, which was prepared by the RF-PECVD method at 150°C in [23], can, in principle, be synthesized by the implantation of carbon ions with an energy of 10 keV into a preheated silicon substrate.

These data demonstrate that the analysis of individual samples after annealing at comparable temperatures provides a lot of information on the structural state and the chemical composition of the layer.

The parameters of the films were determined using X-ray reflectometry with two spectral lines $\text{Cu}K_\alpha$ (0.154 nm) and $\text{Cu}K_\beta$ (0.139 nm). Figure 4 presents the results of X-ray reflectometry of the SiC_x film synthesized by the implantation of carbon ions (40 keV, $3.584 \times 10^{17} \text{ cm}^{-2}$) into silicon after annealing (1300°C, 30 min) on the logarithmic (Fig. 4a) and natural (linear) (Fig. 4b) scales. We did not observe intensity oscillations that could be used to determine the thickness of the film from the distance between their peaks. This is associated with the Gaussian distribution of carbon atoms and with the lack of clear boundaries between layers of different densities. However, the change in density over the depth of the implanted layer can cause intensity fluctuations in the region of the main peak, whose position is used to determine the critical angle of reflection and the density. This can result from the fact that, after the high-dose implantation and annealing, the layer with the Gaussian distribution of carbon atoms (Fig. 1) usually consists of the following layers: the layer of silicon nanocrystals with inclusions of silicon carbide nanocrystals nc -Si + nc -SiC, the nc -SiC layer with nc -Si inclusions, the nc -SiC + nc -Si + nc -C layer, the nc -SiC + nc -Si layer, the nc -Si + nc -SiC layer, and the c -Si substrate. After annealing, the SiO_2 layer can be formed near the surface. For example, Yu Liangdeng et al. [6] showed using the TEM investigations that, after the implantation of C^+ ions with an energy of 80 keV and a dose of $2.7 \times 10^{17} \text{ cm}^{-2}$ into silicon, the sample has a layered structure: defective Si (d -Si), amorphous SiC (a -SiC), 3C-SiC, a -SiC, d -Si, and crystalline Si (c -Si). The annealed sample has a similar layered structure, but amorphous layers (Si, C) are not found.

Indeed, as can be seen from Figs. 4a and 4b, the thin SiC_x layer prepared by the higher dose implantation of carbon ions (40 keV, $3.584 \times 10^{17} \text{ cm}^{-2}$) into silicon is characterized by intensity fluctuations in the region of the main maximum. By extrapolating the intensity curves to $I/2 = 39200 \text{ cps}$ with the Henke program [51], we determined the layer densities of 2.55, 2.90, and 3.29 g/cm^3 (Table 3). This corresponds

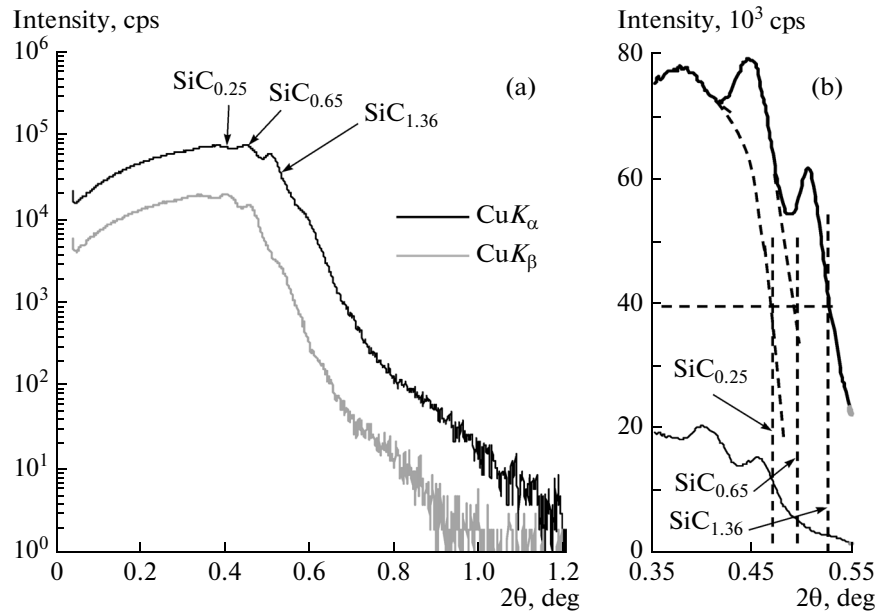


Fig. 4. Results of the $\text{CuK}\alpha$ (0.154 nm) and $\text{CuK}\beta$ (0.139 nm) X-ray reflectometry studies of the SiC_x film synthesized by the C^+ ion implantation (40 keV , $3.584 \times 10^{17} \text{ cm}^{-2}$) into silicon after annealing (1300°C , 30 min) on (a) logarithmic scale and (b) natural scale.

approximately to the density of the subsurface $\text{SiC}_{0.25}$ layer predominantly containing nc -Si nanocrystals with nc -SiC inclusions, the density of the $\text{SiC}_{0.65}$ layer containing nc -SiC with nc -Si inclusions, and the density of the $\text{SiC}_{1.36}$ layer containing nc -SiC with inclusions of ncl -C nanoclusters.

The composition of SiC_x films with the density $\rho_x = 2.55 \text{ g/cm}^3$ was determined according to the formula

$$\rho_x = \rho_1 + (x - x_1)[(\rho_1 - \rho_2)/(x_1 - x_2)]$$

or

$$\rho_y = \rho_1 + (y - y_1)[(\rho_1 - \rho_2)/(y_1 - y_2)], \quad (2)$$

which was derived from the conditions

$$\left(\begin{array}{l} \text{Si} = \text{SiC}_0, \quad x_1 = 0, \quad \rho_1 = 2.33 \text{ g/cm}^3 \\ \text{SiC}_x, \quad 0 < x < 1, \quad 2.33 < \rho_x < 3.21 \text{ g/cm}^3 \\ \text{Si} = \text{SiC}_1, \quad x_2 = 1, \quad \rho_2 = 3.21 \text{ g/cm}^3 \end{array} \right)$$

or

Table 3. X-ray reflectometry determination (using the Henke program [51]) of the density of the SiO_x film synthesized by the carbon ion implantation (40 keV , $3.584 \times 10^{17} \text{ cm}^{-2}$) into silicon after annealing (1300°C , 30 min)

Layer	I_{\max}	$I_{\max}/2$	$2\theta_c$, deg	θ_c , deg	θ_c , mrad	ρ , g cm^{-3}
$\text{SiC}_{0.25}$	78 393	39 200	0.466	0.233	4.067	2.55
$\text{SiC}_{0.65}$	78 393	39 200	0.498	0.249	4.346	2.9
$\text{SiC}_{1.36}$	78 393	39 200	0.529	0.265	4.619	3.29

$$\left(\begin{array}{l} \text{SiC} = \text{Si}_1\text{C}, \quad y_1 = 0, \quad \rho_1 = 3.21 \text{ g/cm}^3 \\ \text{Si}_y\text{C}, \quad 0 < y < 1, \quad 3.21 < \rho_y < 3.51 \text{ g/cm}^3 \\ \text{C} = \text{Si}_0\text{C}, \quad y_2 = 1, \quad \rho_2 = 3.51 \text{ g/cm}^3 \end{array} \right)$$

Here, $x = N_C/N_{\text{Si}}$, $y = N_{\text{Si}}/N_C$, SiC_1 is the silicon carbide of stoichiometric composition, and $\text{SiC}_0 = \text{Si}$. Then, for $x = 0.25$, $x_1 = 0$, $x_2 = 1$ and $\rho_1 = 2.33 \text{ g/cm}^3$, $\rho_2 = 3.21 \text{ g/cm}^3$, from expression (2) we obtain $\rho_x = \rho_{0.25} = 2.55 \text{ g/cm}^3$. For $y = 0.7353$, $y_1 = 1$, $y_2 = 0$ and $\rho_1 = 3.21 \text{ g/cm}^3$, $\rho_2 = 3.51 \text{ g/cm}^3$ (diamond), we obtain $\rho_y = \rho_{0.7353} = 3.29 \text{ g/cm}^3$. In this case, we have $\text{Si}_y\text{C} = \text{SiC}_{1/y}$ or $\text{Si}_{0.7353}\text{C} = \text{SiC}_{1.36}$.

3.2. Ion Implantation Synthesis of Homogeneous Films of Silicon Carbide SiC in Silicon and Investigation of Their Characteristics

In order to obtain homogeneous SiC layers with a rectangular distribution of carbon atoms in silicon (Fig. 1b), the implantation of carbon ions with different energies and doses into silicon was performed in the sequence specified in Table 1. The samples were annealed at 1250°C for 30 min in an argon atmosphere with a low O_2 content. In our previously work [10], we obtained a homogeneous $\text{SiC}_{0.7}$ layer with an increased carbon content near the surface after the implantation and with the SiO_2 layer after annealing.

The IR absorption spectra of the $\text{SiC}_{0.7}$ layer after the ion implantation and annealing at 1250°C for 30 min are shown in Figs. 5 and 6. After the mathe-

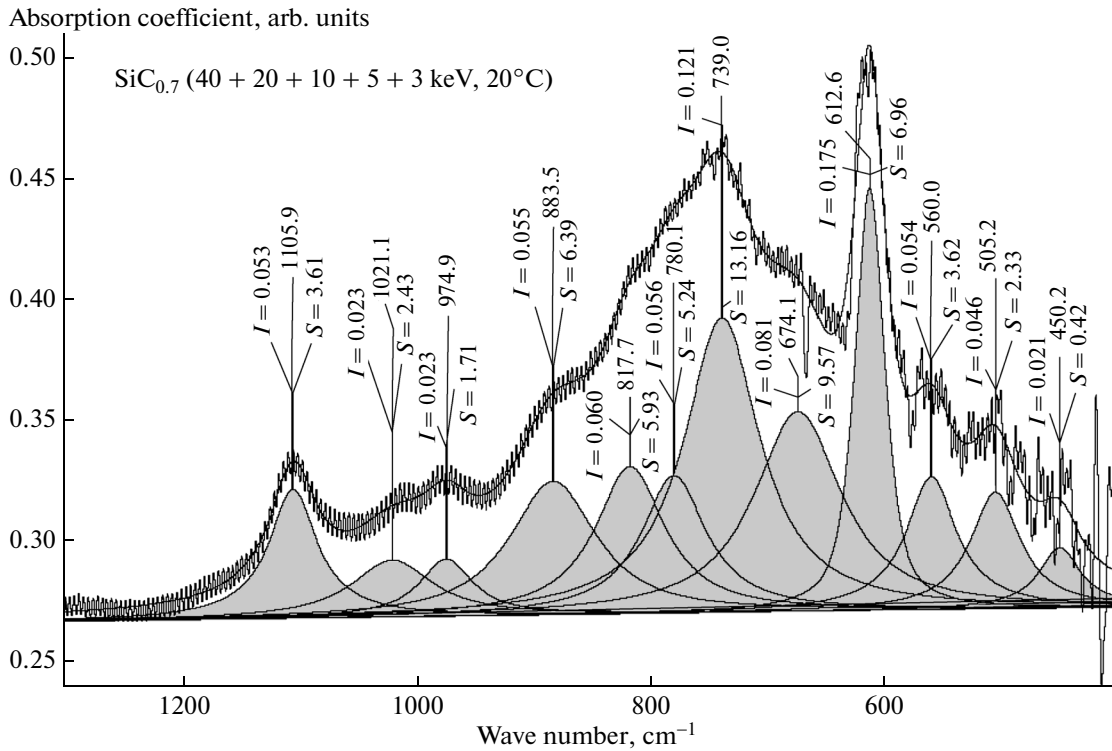


Fig. 5. Mathematical decomposition of the IR absorption spectrum of the SiC_{0.7} layer (Table 4) synthesized by the ion implantation (values at the points of the maxima of the peaks are their amplitudes I , positions, and areas S).

mathematical decomposition, the IR absorption spectrum is represented as the sum of 12 Gaussian components. It is assumed that, after the implantation, the sample contains the molecular complexes SiO₂Si₂ with the characteristic maximum at 1033 cm⁻¹ [48], which are responsible for the appearance of the component with the maximum at 1021.1 cm⁻¹ in the spectrum (Table 4). There is also a component with the maximum at 1105.9 cm⁻¹. This component reflects the presence of interstitial oxygen in the sample [47] and

indicates that the SiO₄ complexes (1100 cm⁻¹) dominate in the oxide layer. After annealing, this component is split into two components with maxima at 1092.6 and 1058 cm⁻¹ due to the transverse optical stretching vibrations of bridging oxygen in the molecular complexes SiO₄ (maximum at 1100 cm⁻¹) and SiO₃Si (maximum at 1067 cm⁻¹) [48]. The total area of these peaks ($S = 20.09$ arb. units) exceeds, by a factor of more than 3, the area of the peaks of the silicon oxide before the annealing ($S = 6.04$ arb. units). This

Table 4. Areas S and sums of the areas $\sum S$ for components of the SiC peak and two components of the SiO peak at wave numbers w

Bond	$T = 20^\circ\text{C}$				$T = 1250^\circ\text{C}$			
	w, cm^{-1}	$S, \text{arb. units}$	$S, \%$	$\sum S, \text{arb. units}$	w, cm^{-1}	$S, \text{arb. units}$	$S, \%$	$\sum S, \text{arb. units}$
Si–O (TO)	1105.9	3.61	59.8	6.04 (100%)	1092.6	9.97	49.6	20.09 (100%)
	1021.1	2.43	40.2		1058.0	10.12	50.4	
Si–C (TO)	883.5	6.39	15.9	40.29 (100%)	884.2	7.09	14.3	49.69 (100%)
	817.7	5.93	14.7		826.5	8.15	16.4	
	780.1	5.24	13.0		795.6	23.95	48.2	
	739.0	13.16	32.7		738.5	8.77	17.6	
	674.1	9.57	23.8		678.7	1.73	3.5	
	612.6	6.96	100.0		6.96	612.3	5.73	

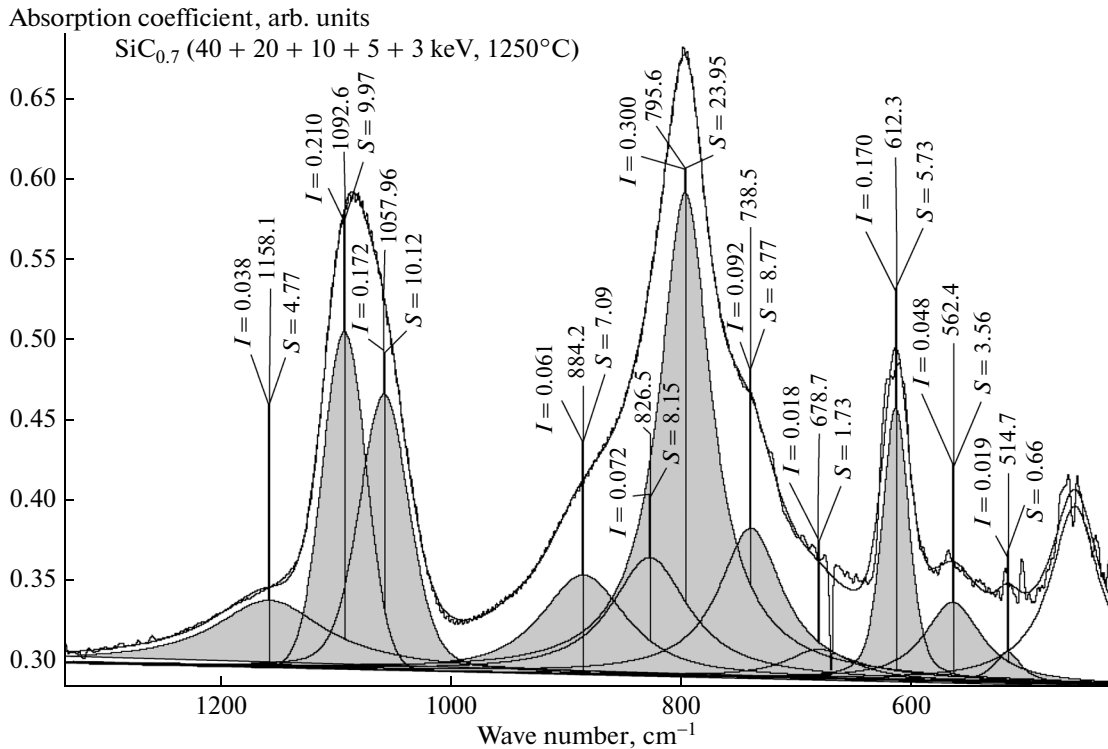


Fig. 6. Mathematical decomposition of the IR absorption spectrum of the SiC_{0.7} layer after the implantation and annealing at 1250°C for 30 min (values at the points of the maxima of the peaks are their amplitudes I , positions, and areas S).

indicates the decomposition of silicon carbide and the oxidation of silicon during the annealing as a result of the interaction with residual oxygen atoms.

The annealing leads to a slight decrease in the area of the component typical of substitutional carbon ($S = 6.96$ and 5.73 arb. units) with the maximum at 612.6 cm^{-1} , which is close to the characteristic value of 607 cm^{-1} [47]. This can be explained by the fact that carbon atoms are embedded in the structure of SiC nanocrystals.

Immediately after the implantation, the absence of the component at 794 cm^{-1} and the position of the resulting maximum at 739 cm^{-1} indicate a noncrystalline nature of the implanted layer. After annealing at 1250°C , the total number of Si–C bonds (Table 4) increases by 23% due to the decomposition of optically inactive stable clusters and their transformation into optically active Si–C bonds. The maximum of the peak attributed to SiC is shifted to the value of 795.6 cm^{-1} . This suggests that the tetrahedrally oriented Si–C bonds dominate in the layer after annealing.

In actual fact, Yu Liangdeng et al. [6, p. 73] observed that, after the implantation of C ions with an energy of 80 keV and a dose of 2.7×10^{17} cm^{-2} into silicon, the IR absorption spectrum contains a broad Gaussian band centered at 700 cm^{-1} due to the presence of amorphous SiC inclusions in the sample. The Lorentzian contribution of the spectral component of

crystalline β -SiC at 796.2 cm^{-1} appears only after annealing. Borders et al. [8] revealed that, after the $^{12}\text{C}^+$ implantation ($E = 200$ keV, $D \approx 10^{17}$ cm^{-2}), the IR spectrum contains a broad absorption band centered at 700 – 725 cm^{-1} . After annealing at 825°C , this band is shifted to 800 cm^{-1} , which corresponds to the transverse optical phonon absorption band of SiC. The observed decrease in the half-width of this peak at temperatures of $850 \pm 25^\circ\text{C}$ indicates the formation of crystalline SiC. Baranova et al. [26] synthesized crystalline SiC films by the implantation of C^+ ions ($E = 40$ keV, $D > 10^{17}$ cm^{-2}) into silicon wafers. At temperatures of 600 – 700°C , these authors observed a change in the position of the absorption maximum from 715 to 815 cm^{-1} . Chen et al. [52] prepared the buried SiC layers by the implantation of C^+ ions with energies of 40 and 65 keV into p -Si. After annealing of the layers at 600 – 1200°C , they decomposed the FT-IR spectrum into three Gaussian components, one of which with the maximum at 700 cm^{-1} was attributed to amorphous SiC and the other two components with higher (larger grains) and lower (smaller grains) FWHM values and with the maximum at 795 ± 1 cm^{-1} were assigned to β -SiC. After annealing, the total area of the spectra (or the amount of the formed SiC layers) increased; i.e., before annealing, not all carbon atoms in samples were bound to the Si atoms.

The ratio of weak elongated Si–C bonds (components at 739.0 and 674.1 cm^{-1}) of the amorphous phase, strong shortened Si–C bonds (components at 817.7 and 883.5 cm^{-1}) on the surface of small nanocrystals, and tetrahedral Si–C bonds of the crystalline phase (degree of crystallinity) is equal to 22.7/12.3/5.24 (or 56/31/13%) after the implantation and 10.5/15.2/24.0 (or 21/31/48%) after annealing. The degree of crystallinity of the layer, which is determined as the fraction of bonds that are close to the tetrahedral orientation, amounts to 13% before annealing and 48% after annealing (Table 4). The observed shift of the maximum is favored by a decrease in the content of the amorphous part of the layer from 56 to 21% and by an increase in the content of nanocrystals from 13 to 48% while retaining the same number of short bonds on the surface of small nanocrystals (31%).

The small fraction of tetrahedrally oriented Si–C bonds (48%) in the $\text{SiC}_{0.7}$ layer, which is an intermediate value between the degrees of crystallinity of the inhomogeneous layers produced by the implantation of carbon ions with energies of 10 (42%) and 40 (71%) keV into silicon, is due to an increased concentration of stable carbon clusters, because the average carbon concentration $N_C/N_{\text{Si}} = 0.7$ is significantly higher than that in the layer prepared by the implantation of carbon ions with an energy of 40 keV (Fig. 1).

The high content of the amorphous component (21%) after annealing at 1250°C for layers with a carbon concentration lower than the concentration corresponding to stoichiometric SiC can seem questionable. For example, Kimura et al. [49] showed that all the implanted carbon atoms are incorporated into β -SiC during the annealing at temperatures of 900–1200°C, provided that the concentration of carbon atoms does not exceed the concentration corresponding to the stoichiometric composition of β -SiC at the maximum of the distribution. At higher implantation doses, excess carbon atoms form clusters and are not embedded in β -SiC even after annealing at 1200°C. Calcagno et al. [42] prepared the $\text{Si}_{1-x}\text{C}_x$ alloys in silicon by multiple implantation of C^+ ions with doses in the range from 5×10^{16} to $3 \times 10^{17} \text{ cm}^{-2}$ and energies in the range of 10–30 keV. After annealing of the sample at 1000°C, the authors observed a shift in the peak of the IR signal toward the 795 cm^{-1} and its narrowing, which indicated the formation of the crystalline SiC phase. The TEM and X-ray diffraction investigations revealed the formation of β -SiC crystallites with sizes in the range of 5–10 nm, which was also observed by other authors [53, 54]. Only an increase in the carbon concentration ($x > 0.55$) led to the formation of carbon inclusions ($\sim 2.5 \text{ nm}$) in the sample. Nonetheless, we assume that carbon clusters of smaller sizes can also be formed at the carbon concentration below the concentration corresponding to the stoichiometric SiC composition. For example, in [8], the decrease in the half-width of the SiC peak in the IR absorption spec-

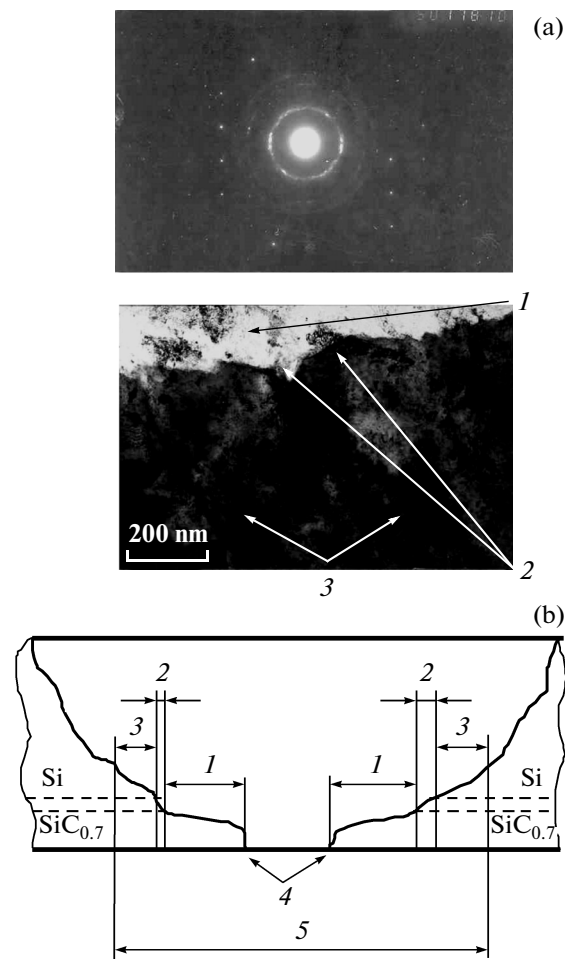


Fig. 7. Transmission electron diffraction pattern and microstructure ($\times 50000$) of the multiply $^{12}\text{C}^+$ -implanted silicon layers on the “ $\text{SiC}_{0.7}$ layer + transition layer + c -Si” regions after annealing at 1200°C for 30 min. (a) SiC (rings), Si (point reflections), $\text{SiC}_{0.7}$ (bright areas), and c -Si (dark areas). (b) Schematic cross section of the studied sample: (1) $\text{SiC}_{0.7}$ regions, (2) Si– $\text{SiC}_{0.7}$ transition layer regions, (3) double diffraction regions, (4) through hole, and (5) transmitted region.

trum after the $^{12}\text{C}^+$ implantation ($E = 200 \text{ keV}$, $D \approx 10^{17} \text{ cm}^{-2}$) and annealing at temperatures of $850 \pm 25^\circ\text{C}$ indicated the formation of crystalline SiC; however, it was concluded that only about half of the carbon atoms are included in SiC.

The high-dose implantation of carbon ions into silicon leads to a change in the composition and to an increase in the density of the subsurface layer. In turn, the increase in the density of the layer during the implantation leads to a decrease in the projected range R_p and the root-mean-square deviation ΔR_p . The decrease in ΔR_p leads to the formation of a more abrupt boundary between the SiC film and Si substrate. Therefore, we can assume that the X-ray reflectometry method can be used to measure the thickness and density of the $\text{SiC}_{0.7}$ film. Indeed, the TEM inves-

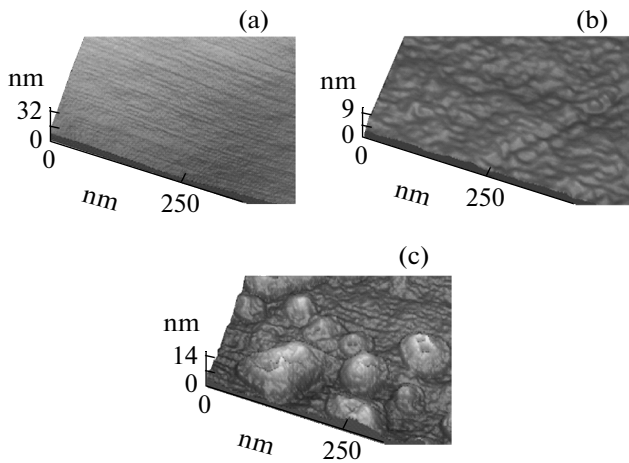


Fig. 8. Surface topography of the $\text{SiC}_{0.7}$ layer: (a) after multiple implantation of carbon ions with energies of 40, 20, 10, 5, and 3 keV into silicon and (b, c) after annealing for 30 min at temperatures $T =$ (b) 800 and (c) 1250°C.

tigations of two samples (Fig. 7a) revealed a sharp transition between the $\text{SiC}_{0.7}$ film and the Si substrate in the form of a clear boundary between the bright (the $\text{SiC}_{0.7}$ layer) and dark (the Si substrate) regions.

The superposition of the point and ring electron diffraction patterns (Fig. 7a) is observed in the patterns from sections 3, in which the studied objects are

brought into coincidence with single-crystal and polycrystalline structures ($\text{Si} + \text{SiC}_{0.7}$). The region under investigation can be divided into three parts (Fig. 7b): section 1 is the $\text{SiC}_{0.7}$ layer; section 2 is the $\text{SiC}_{0.7}$ layer + Si– $\text{SiC}_{0.7}$ transition layer; and section 3 is the $\text{SiC}_{0.7}$ layer + Si– $\text{SiC}_{0.7}$ transition layer + c -Si layer. In the transition layer, a decrease in the concentration of carbon atoms leads to the fact that, during the high-temperature recrystallization, excess silicon atoms located between large SiC grains are embedded in the substrate, thus forming a sawtooth SiC–Si structure (Fig. 7a). The crystallographic structure of the samples was investigated by analyzing the ring electron diffraction patterns. It was found that the experimentally measured diameters of the rings in the electron diffraction pattern are in good agreement with the calculated diameters of the rings formed for the face-centered cubic lattice β -SiC due to the reflection from planes with the indices (111), (220), (311), (222), (331), and (422).

The atomic force microscopy revealed (Fig. 8) that, after the implantation and annealing at temperatures of 800 and 1250°C for 30 min, the layer has a smooth surface with fluctuations within 9–14 nm. The formation of grains does not lead to a significant deformation of the surface. This can also favor the appearance of intensity oscillations in the X-ray reflectometry measurement of the layer parameters.

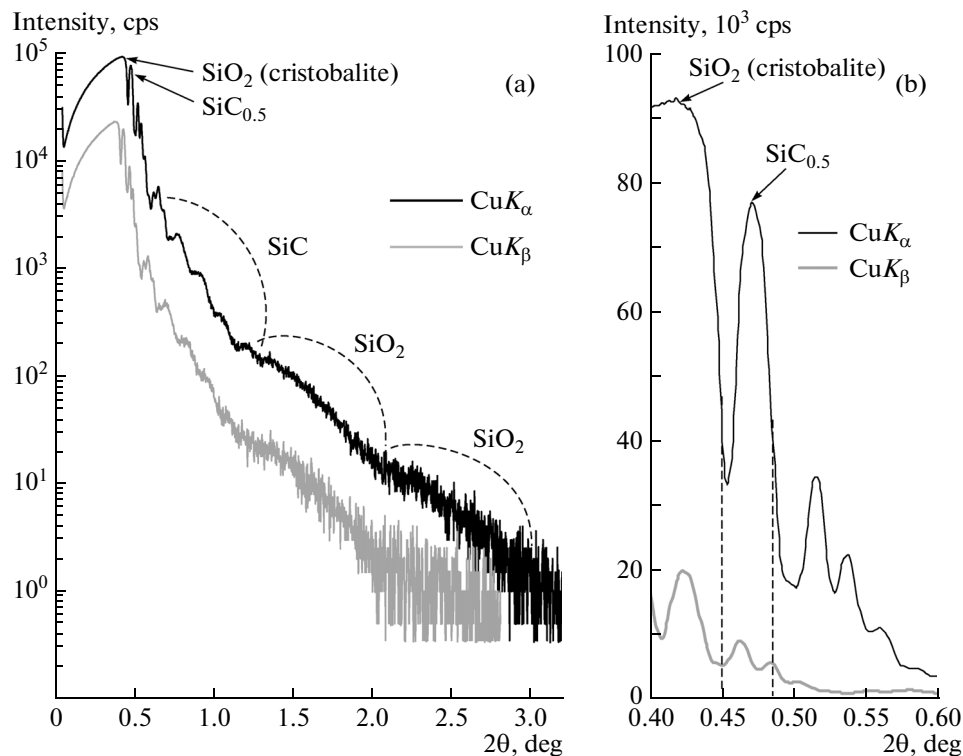


Fig. 9. Results of the CuK_α (0.154 nm) and CuK_β (0.139 nm) X-ray reflectometry studies of the $\text{SiC}_{0.7}$ film on silicon after annealing at 1250°C on (a) logarithmic scale and (b) natural scale.

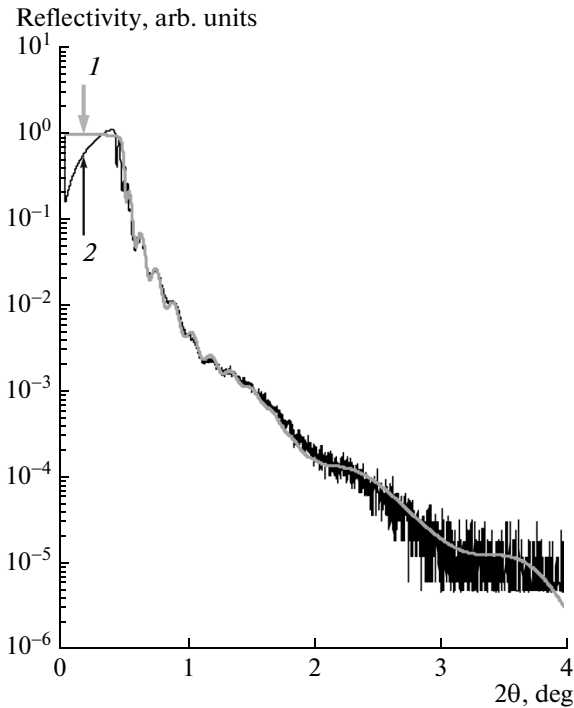


Fig. 10. (1) Calculated curve simulated with the Release software [18] and (2) experimental X-ray reflectometry curve of the $\text{SiC}_{0.7}$ films after annealing at 1250°C .

We revealed intensity oscillations attributed to the interference of X-ray reflections in the $\text{SiC}_{0.7}$ and SiO_2 layers (Fig. 9a). The first reflection maximum with the intensity $I_1 = 93207$ cps is observed at $2\theta = 0.418^\circ$. The angle of the total external reflection was estimated as the angle where the reflection intensity is approximately equal to half the maximum $I = I_1/2 = 46603$ cps, i.e., $2\theta_c = 0.449^\circ$ (Fig. 9b) or $\theta_c = 0.2245^\circ = 3.918$ mrad. Using the Henke program [51], we determined that this value of θ_c corresponds to the density of the film (2.37 g/cm³) and is close to the density of cristobalite SiO_2 (2.32 g/cm³). Then, with an increase in the angle of incidence, the reflection intensity again increases to $I_2 = 76831$ cps and indicates a more dense structure. A further decrease in the intensity to $I_2/2 = 38415$ cps occurs at $2\theta_c = 0.486^\circ$ (Fig. 9b) or $\theta_c = 0.243^\circ = 4.241$ mrad, which corresponds to the density of 2.77 g/cm³ and is close to the density of quartz (2.65 g/cm³) or $\text{SiC}_{0.5}$ (2.77 g/cm³). Further, we observe again an increase in the intensity from 17298 to $I_3 = 34416$ cps (Fig. 9b) and, then, a continuous decrease to the appearance of oscillations.

Using the simulation with the Release software [55], we obtained a theoretical curve that is closely similar to the experimental curve (Fig. 10) and corresponds to the main parameters of the following systems:

- (1) the $\text{SiC}_{2.0}$ layer (thickness $d = 2.0$ nm, density $\rho = 3.26$ g/cm³, surface roughness $\sigma = 0.44$ nm),
- (2) the SiO_2 layer ($d = 5.3$ nm, $\rho = 2.88$ g/cm³, $\sigma = 1.1$ nm),
- (3) the $\text{SiC}_{0.8}$ layer ($d = 1.5$ nm, $\rho = 3.03$ g/cm³, $\sigma = 0$ nm),
- (4) the $\text{SiC}_{0.6}$ layer ($d = 43.7$ nm, $\rho = 2.85$ g/cm³, $\sigma = 0$ nm),
- (5) the Si substrate ($\rho = 2.33$ g/cm³, $\sigma = 1.8$ nm).

The total layer thickness proves to be equal to 52.5 nm, which is less than the expected value. This can be associated with the effect of sputtering in the high-dose carbon ion implantation into silicon.

4. CONCLUSIONS

The structure and composition of ion-implanted (with energies of 10 and 40 keV) silicon subsurface layers with a Gaussian distribution profile of carbon atoms in silicon, as well as with a rectangular profile ($\text{SiC}_{0.7}$), were investigated. It was assumed that, in the homogeneous $\text{SiC}_{0.7}$ layer after the annealing, the structural–phase composition does not change over the depth, whereas in inhomogeneous layers with a Gaussian distribution profile of carbon atoms, not only the concentrations of C and Si atoms but also, as a consequence, the concentrations of nanocrystals and nanoclusters of Si, SiC, and C change over the depth.

The mathematical decomposition of the IR absorption spectrum of the $\text{SiC}_{0.7}$ film was carried out. Based on the proportionality between the area of the spectral component and the number of the corresponding Si–C bonds, we determined the areas S before and after the annealing at 1250°C for 12 spectral components, including components with maxima in the following positions: 612 cm^{−1} (carbon in substitutional sites); 739 , 674 , and 678 cm^{−1} (weak elongated Si–C bonds in amorphous silicon carbide); 780 cm^{−1} (Si–C bonds close to the tetrahedral orientation); 795 cm^{−1} (Si–C bonds close to tetrahedral orientation of crystalline SiC); and 817 , 826 , and 884 cm^{−1} (shortened Si–C bonds). It was shown that, immediately after the implantation, the absence of the component at 794 cm^{−1} and the position of the resulting maximum at 739 cm^{−1} indicate a noncrystalline nature of the implanted layer. After the annealing at 1250°C , the total number of optically active Si–C bonds increased by 23% due to the decomposition of optically inactive stable clusters. Before and after the annealing, the ratios of the numbers of weak elongated Si–C bonds of the amorphous phase, strong shortened Si–C bonds on the surface of small nanocrystals, and tetrahedral Si–C bonds of the crystalline phase (degree of crystallinity) were equal to 56/31/13 and 21/31/48%, respectively.

It was demonstrated that there is an abrupt boundary between the SiC_{0.7} film and the Si substrate. After the implantation and annealing at 1250°C, the layer had a smooth surface with fluctuations within 9–14 nm, and the formation of grains did not lead to a significant deformation of the surface. The intensity oscillations revealed by X-ray reflectometry were attributed to the interference of X-ray reflections in the layers of SiC_{0.7} and SiO₂. Using the simulation with the Release software, we obtained a theoretical curve, which is closely similar to the experimental curve and corresponds to the main parameters of the following systems: (1) the SiC_{2.0} layer (thickness $d = 2.0$ nm, density $\rho = 3.26$ g/cm³, surface roughness $\sigma = 0.44$ nm), (2) the SiO₂ layer ($d = 5.3$ nm, $\rho = 2.88$ g/cm³, $\sigma = 1.1$ nm), (3) the SiC_{0.8} layer ($d = 1.5$ nm, $\rho = 3.03$ g/cm³, $\sigma = 0$ nm), (4) the SiC_{0.6} layer ($d = 43.7$ nm, $\rho = 2.85$ g/cm³, $\sigma = 0$ nm), and (5) the Si substrate ($\rho = 2.33$ g/cm³, $\sigma = 1.8$ nm).

For inhomogeneous subsurface silicon layers with a Gaussian distribution profile of carbon atoms in silicon, which were synthesized by the carbon ion implantation with the parameters $E = 40$ keV, $D = 3.56 \times 10^{17}$ cm⁻² and $E = 10$ keV, $D = 1.56 \times 10^{17}$ cm⁻², followed by annealing for 30 min at temperatures of 1300 and 1400°C, respectively, the total numbers of optically active Si–C bonds were found to be almost identical to each other, although there are significant differences in the ion energies and doses because the annealing temperatures differ by 100°C near the melting point of silicon.

The mathematical decomposition of the IR absorption spectrum obtained from a silicon layer after the ion implantation with energies of 10 and 40 keV demonstrated that fractions of weak elongated Si–C bonds in the amorphous phase, strong shortened Si–C bonds on the surface of small nanocrystals, and tetrahedral Si–C bonds in the crystalline phase (degree of crystallinity) after high-temperature annealing of the layers are equal to 11.5/11.4/16.8 and 8.7/2.5/27.9 (or 29/29/42 and 22/7/71%), respectively.

It was shown that the low degree of crystallinity (42%) of the layer synthesized by the implantation of 10-keV carbon ions into silicon is associated with the sputtering effects and the higher concentration of carbon atoms and stable carbon clusters, whose decomposition at a high temperature of 1400°C led to the formation of small-sized SiC nanocrystals with a high fraction of shortened Si–C bonds on their surface.

After the high-temperature annealing (1300°C), the high degree of crystallinity (71%) of the silicon layer implanted by C⁺ ions with an energy of 40 keV, as compared to the degree of crystallinity (48%) of the SiC_{0.7} layer or the degree of crystallinity (42%) of the layer after the C⁺ ion implantation with an energy of 10 keV, was explained by the lower average concentra-

tion of carbon and stable carbon clusters after the implantation.

The X-ray reflectometry data on fluctuations of the intensity of X-ray reflections in the region of the main maximum were interpreted in terms of variations in the density over the depth of the layer with a Gaussian distribution of carbon atoms (40 keV). Using the Henke program, we identified the SiC_{0.25} layer (silicon nanocrystals *nc*-Si with *nc*-SiC inclusions, $\rho = 2.55$ g/cm³), the SiC_{0.65} layer (*nc*-SiC with *nc*-Si inclusions, 2.90 g/cm³), and the SiC_{1.36} layer (*nc*-SiC with *ncl*-C inclusions, 3.29 g/cm³).

ACKNOWLEDGMENTS

This study was supported by the Committee of Science of the Ministry of Education and Science of the Republic of Kazakhstan within the framework of the program “Investigation of Nanostructured Silicon Carbide Layers Synthesized by Ion Implantation and Ion Beam Sputtering” (grant no. GR 0217/GF, 2012–2014, priority “Intellectual Potential of the Country,” subpriority “Basic Research in the Field of Natural Sciences”).

REFERENCES

1. F. Liao, S. L. Girshick, W. M. Mook, W. W. Gerberich, and M. R. Zachariah, *Appl. Phys. Lett.* **86**, 171913 (2005).
2. A. V. Afanas'ev, V. A. Il'in, A. V. Korlyakov, A. O. Lebedev, V. V. Luchinin, and Yu. M. Tairov, in *Physics and Technology of Micro- and Nanosystems*, Ed. by V. V. Luchinin and V. V. Malinovskii (Russkaya Kolleksiya, St. Petersburg, 2011), p. 50.
3. K. Oguri and T. Sekigawa, US Patent No. 2004/0180242 A1 (2004).
4. H. Yan, B. Wang, X. M. Song, L. W. Tan, S. J. Zhang, G. H. Chen, S. P. Wong, R. W. M. Kwok, and W. M. L. Leo, *Diamond Related Mater.* **9**, 1795 (2000).
5. D. Chen, S. P. Wong, Sh. Yang, and D. Mo, *Thin Solid Films* **426**, 1 (2003).
6. Yu Liangdeng, Saweat Intarasiri, Teerasak Kamwanna, and Somsorn Singkarat, in *Ion Beam Applications in Surface and Bulk Modification of Insulators* (International Atomic Energy Agency, Vienna, Austria, 2008), p. 63.
7. J. K. N. Lindner, *Appl. Phys. A* **77**, 27 (2003).
8. J. A. Borders, S. T. Picraux, and W. Beezhold, *Appl. Phys. Lett.* **18** (11), 509 (1971).
9. R. M. Bayazitov, I. B. Haibullin, R. I. Batalov, R. M. Nurutdinov, L. Kh. Antonova, V. P. Aksenov, and G. N. Mikhailova, *Nucl. Instrum. Methods Phys. Res., Sect. B* **206**, 984 (2003).
10. K. Kh. Nussupov and N. B. Beisenkhanov, in *Silicon Carbide-Materials, Processing and Applications in Electronic Devices*, Ed. by M. Mukherjee (InTech, Rijeka, Croatia, 2011), Chap. 4, p. 69.
11. K. Kh. Nusupov, N. B. Beisenkhanov, I. V. Valitova, E. A. Dmitrieva, D. Zhumagaliuly, and E. A. Shilenko, *Phys. Solid State* **48** (7), 1255 (2006).

12. J. Zhao, D. S. Mao, Z. X. Lin, B. Y. Jiang, Y. H. Yu, X. H. Liu, H. Z. Wang, and G. O. Yang, *Appl. Phys. Lett.* **73** (13), 1838 (1998).
13. D. I. Tetelbaum, A. N. Mikhaylov, A. I. Belov, V. K. Vasiliev, A. I. Kovalev, D. L. Wainshtein, Y. Golan, and A. Osherov, *J. Surf. Invest.: X-Ray, Synchrotron Neutron Tech.* **3** (5), 702 (2009).
14. L. Pavesi, *Mater. Today* **8** (1), 18 (2005).
15. A. Perez-Rodriguez, O. Gonzalez-Varona, B. Garrido, P. Pellegrino, J. R. Morante, C. Bonafos, M. Carrada, and A. Claverie, *J. Appl. Phys.* **94** (1), 254 (2003).
16. O. Gonzalez-Varona, A. Perez-Rodriguez, B. Garrido, C. Bonafos, M. Lopez, J. R. Morante, J. Montserrat, and R. Rodriguez, *Nucl. Instrum. Methods Phys. Res., Sect. B* **161–163**, 904 (2000).
17. A. I. Belov, A. N. Mikhailov, D. E. Nikolichiev, A. V. Boryakov, A. P. Sidorin, A. P. Grachev, A. V. Ershov, and D. I. Telebaum, *Semiconductors* **44** (11), 1450 (2010).
18. G. Conibeer, M. Green, R. Corkish, Y. Cho, E. Cho, C. Jiang, T. Fangsuwannarak, E. Pink, Y. Huang, T. Puzzer, T. Trupke, B. Richards, A. Shalav, and K. Lin, *Thin Solid Films* **511–512**, 654 (2006).
19. G. P. Yarovoi, N. V. Latukhina, A. S. Rogozhin, A. S. Gurto, S. V. Ivkov, and S. I. Minenko, *Izv. Samar. Nauchn. Tsentra, Ross. Akad. Nauk* **14** (1), 521 (2012).
20. T. Chen, Y. Huang, A. Dasgupta, M. Luysberg, L. Houben, D. Yang, R. Carius, and F. Finger, *Sol. Energy Mater. Sol. Cells* **98**, 370 (2012).
21. T. Chen, Y. Huang, H. Wang, D. Yang, A. Dasgupta, R. Carius, and F. Finger, *Thin Solid Films* **517** (12), 3513 (2009).
22. S. Ogawa, M. Okabe, Y. Ikeda, T. Itoh, N. Yoshida, and S. Nonomura, *Thin Solid Films* **516** (5), 740 (2008).
23. J. Ma, J. Ni, J. Zhang, Z. Huang, G. Hou, X. Chen, X. Zhang, X. Geng, and Y. Zhao, *Sol. Energy Mater. Sol. Cells* **114**, 9 (2013).
24. D. Pysch, M. Bivour, M. Hermle, and S. W. Glunz, *Thin Solid Films* **519** (8), 2550 (2011).
25. N. I. Klyui, V. G. Litovchenko, A. G. Rozhin, V. N. Dikusha, M. Kittler, and W. Seifert, *Sol. Energy Mater. Sol. Cells* **72** (1–4), 597 (2002).
26. E. K. Baranova, K. D. Demakov, K. V. Starinin, L. N. Strel'tsov, and I. B. Khaibullin, *Dokl. Akad. Nauk SSSR* **200**, 869 (1971).
27. T. Kimura, Sh. Kagiya, and Sh. Yugo, *Thin Solid Films* **122**, 165 (1984).
28. I. P. Akimchenko, K. V. Kisseleva, V. V. Krasnopevtsev, Yu. V. Milyutin, A. G. Touryanski, V. S. Vavilov, *Radiat. Eff.* **33**, 75 (1977).
29. K. Kh. Nusupov, *Extended Abstract of Doctoral Dissertation (Lebedev Physical Institute, Russian Academy of Sciences, Moscow, 1996)*.
30. I. P. Akimchenko, Kh. R. Kazdaev, I. A. Kamenskikh, and V. V. Krasnopevtsev, *Sov. Phys. Semicond.* **13** (2), 219 (1979).
31. T. Kimura, Sh. Kagiya, and Sh. Yugo, *Thin Solid Films* **81** (4), 319 (1981).
32. K. Srikanth, M. Chu, S. Ashok, N. Nguyen, and K. Vedam, *Thin Solid Films* **163**, 323 (1988).
33. N. N. Gerasimenko, O. N. Kuznetsov, L. V. Lezheiko, E. V. Lyubopytova, L. S. Smirnov, and F. L. Edel'man, *Mikroelektronika* **3** (5), 467 (1974).
34. I. P. Akimchenko, K. V. Kisseleva, V. V. Krasnopevtsev, A. G. Touryanski, and V. S. Vavilov, *Radiat. Eff.* **48**, 7 (1980).
35. R. M. Bayazitov, I. B. Khaibullin, R. I. Batalov, and R. M. Nurutdinov, *Tech. Phys.* **48** (6), 742 (2003).
36. K. V. Vaidyanathan, *J. Appl. Phys.* **44** (2), 583 (1973).
37. M. J. Koyama, *J. Appl. Phys.* **51** (6), 3202 (1980).
38. M. Reeson, J. Stoemenos, and P. L. F. Hemment, *Thin Solid Films* **191**, 147 (1990).
39. K. Kh. Nussupov, V. O. Sigle, and N. B. Beisenkhanov, *Nucl. Instrum. Methods Phys. Res., Sect. B* **82**, 69 (1993).
40. P. Durupt, B. Canut, J. P. Gauthier, J. A. Roger, and J. Pivot, *Mater. Res. Bull.* **15**, 1557 (1980).
41. I. P. Akimchenko, Kh. R. Kazdaev, and V. V. Krasnopevtsev, *Sov. Phys. Semicond.* **11** (10), 1149 (1977).
42. L. Calcagno, G. Compagnini, G. Foti, M. G. Grimaldi, and P. Musumeci, *Nucl. Instrum. Methods Phys. Res., Sect. B* **120** (1), 121 (1996).
43. W. Rothmund and C. R. Fritzsche, *J. Electrochem. Soc.* **121**, 4, 586 (1974).
44. A. G. Touryanski, A. V. Vinogradov, and I. V. Pirshin, *US Patent No. 6 041 098* (2000).
45. A. Tur'yanskii, N. Gerasimenko, I. Pirshin, and V. Senkov, *Nanoindustriya* **5**, 40 (2009).
46. J. F. Gibbons, W. S. Johnson, and S. W. Mylroie, *Projected Range Statistics: Semiconductors and Related Materials*, 2nd ed. (Dowden, Hutchinson and Ross, Stroudsburg, 1975).
47. D. I. Brinkevich, N. V. Vabishchevich, and V. S. Proselovich, *Vestn. Belarus. Gos. Univ., Ser. 1: Fiz., Mat. Inform., No. 1*, 41 (2010).
48. I. P. Lisovskyy, I. Z. Indutnyy, B. N. Gnenny, P. M. Lytvyn, D. O. Mazunov, A. S. Oberemok, N. V. Sopinskyy, and P. E. Shepelyavyi, *Semiconductors* **37** (1), 97 (2003).
49. T. Kimura, Sh. Kagiya, and Sh. Yugo, *Thin Solid Films* **94**, 191 (1982).
50. S. P. Wong, D. Chen, L. C. Ho, H. Yan, and R. W. M. Kwok, *Nucl. Instrum. Methods Phys. Res., Sect. B* **140** (1–2), 70 (1998).
51. B. L. Henke, E. M. Gullikson, and J. C. Davis, *At. Data Nucl. Data Tabl.* **54** (2), 181 (1993). http://henke.lbl.gov/optical_constants/.
52. D. Chen, W. Y. Cheung, and S. P. Wong, *Nucl. Instrum. Methods Phys. Res., Sect. B* **148** (1–4), 589 (1999).
53. J. K. N. Lindner, K. Volz, U. Preckwinkel, B. Gotz, A. Frohnwieser, B. Stritzker, and B. Rauschenbach, *Mater. Chem. Phys.* **46** (2–3), 147 (1996).
54. P. Martin, B. Daudin, M. Dupuy, A. Ermolieff, M. Olivier, A. M. Papon, and G. J. Rolland, *J. Appl. Phys.* **67** (6), 2908 (1990).
55. S. A. Aprelov, *Extended Abstract of Candidate's Dissertation (Moscow State Institute of Electronic Technology, Moscow, 2007)*.

Translated by O. Borovik-Romanova